CDDpress

www.nature.com/cddis

CORRECTION OPEN

Check for updates

Correction: Smooth muscle 22 alpha protein inhibits VSMC foam cell formation by supporting normal LXRα signaling, ameliorating atherosclerosis

Dan-Dan Zhang, Yu Song, Peng Kong, Xin Xu, Ya-Kun Gao, Yong-Qing Dou, Lin Weng, Xiao-Wei Wang, Yan-Ling Lin, Fan Zhang, Hailin Zhang and Mei Han

Cell Death and Disease (2021)12:1071 ; https://doi.org/10.1038/s41419-021-04360-w

Correction to: *Cell Death and Disease* https://doi.org/10.1038/s41419-021-04239-w, published online 22 October 2021

The original version of this article unfortunately contained a mistake. Due to a typesetting error some of the figures were omitted and figure legends were misplaced. We sincerely apologize for the errors. The correct figures and legends can be found below.

Published online: 10 November 2021

Official journal of CDDpress

SPRINGER NATURE
CDDpress

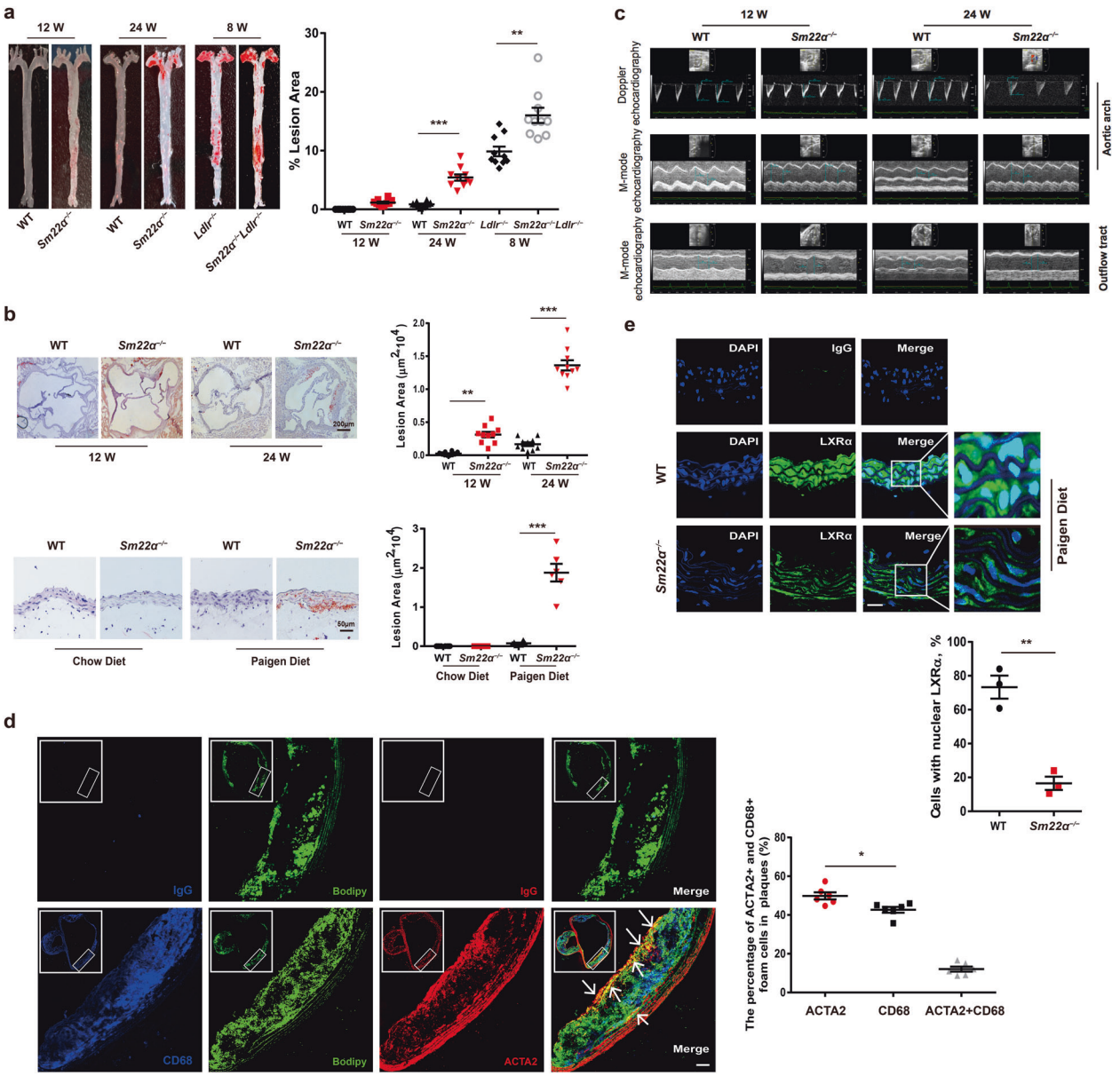

Fig. 1 Impaired SM22α expression is associated with development of atherosclerosis. a, **b** WT ($n = 10$) and *Sm22a*$^{-/-}$ ($n = 10$) mice with or without *Ldlr*$^{-/-}$ background ($n = 10$) fed Paigen diet for 8, 12, and 24 weeks, respectively. Representative images of *en face* ORO-stained aortas (**a**), aortic sinus, aortic cross sections (**b**), and quantification of lesion areas are shown. **c** M-mode and Doppler echocardiography images obtained from aortic arch and outflow tract of WT ($n = 15$) and *Sm22a*$^{-/-}$ ($n = 15$) mice fed Paigen diet for 12 and 24 weeks. A_s: outflow tract and aortic diameter in systole; A_d: outflow tract and aortic diameter in diastole. **d** Identification of SMC-derived foam cells within atherosclerotic lesion of *Sm22a*$^{-/-}$ mice ($n = 6$) by CD68 (blue), ACTA2 (red), and Bodipy (green). Scale bar, 20 μm. Arrows indicated foam cells, which were VSMCs-derived. **e** Representative immunofluorescence of LXRα (red) and quantification of cells with nuclear LXRα in the aortic sections from WT ($n = 3$) and *Sm22a*$^{-/-}$ ($n = 3$) mice. Scale bar, 15 μm. Data and images are representative of at least three independent experiments. Data in **a** and **b** were analyzed by two-way and one-way ANOVA, respectively. Data in **d** and **e** were analyzed by unpaired *t*-test. *$p < 0.05$; **$p < 0.01$; ***$p < 0.001$.

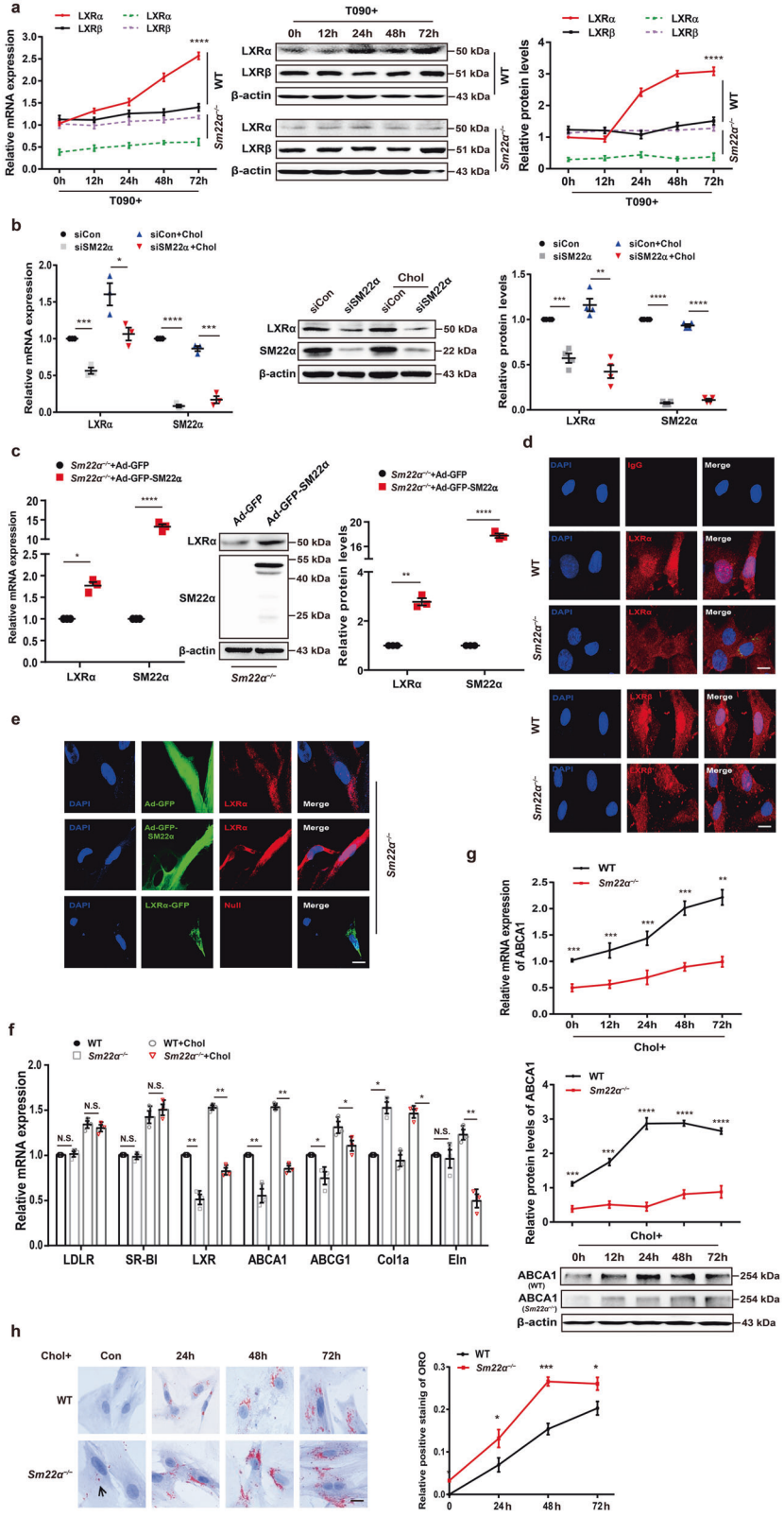
a
LXRα
LXRβ
Relative mRNA expression
T090+
0h 12h 24h 48h 72h
WT
Sm22α−/−
β-actin
50 kDa
51 kDa
43 kDa
Relative protein levels
b
siCon
siSM22α
siCon+Chol
siSM22α+Chol
Chol
SM22α
22 kDa
c
Sm22α−/−+Ad-GFP
Sm22α−/−+Ad-GFP-SM22α
Ad-GFP
Ad-GFP-SM22α
55 kDa
40 kDa
25 kDa
d
DAPI
IgG
Merge
e
Ad-GFP
Ad-GFP-SM22α
LXRα-GFP
Null
f
WT
WT+Chol
Sm22α−/−+Chol
N.S.
LDLR
SR-BI
LXR
ABCA1
ABCG1
Col1a
Eln
g
Relative mRNA expression of ABCA1
Chol+
Relative protein levels of ABCA1
ABCA1 (WT)
ABCA1 (Sm22α−/−)
254 kDa
h
Con
24h
48h
72h
Relative positive staining of ORO

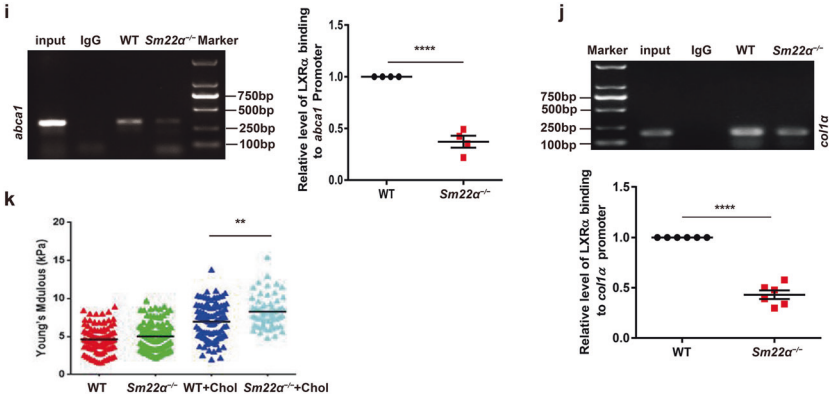

Fig. 2 Expression and activity of LXRα is abnormal in *Sm22α*$^{-/-}$ VSMCs. **a** qRT-PCR and Western blot analysis of LXRα and LXRβ in WT and *Sm22α*$^{-/-}$ VSMCs treated with LXRs agonist T090 for 0, 12, 24, 48, and 72 h, respectively, ($n = 3$). **b** qRT-PCR and western blot analysis of LXRα in WT VSMCs with or without cholesterol loading following knockdown of SM22α ($n = 3$). **c** qRT-PCR and western blot analysis of LXRα and SM22α expression in *Sm22α*$^{-/-}$ VSMCs transducted with Ad-GFP and Ad-GFP-SM22α for 24 h ($n = 3$). **d** Confocal microscopy images of LXRα and LXRβ distribution in WT and *Sm22α*$^{-/-}$ VSMCs. Scale bar, 10 μm. **e** Immunofluorescence staining for endogenous LXRα and LXRα-GFP in *Sm22α*$^{-/-}$ VSMCs transducted with Ad-GFP and Ad-GFP-SM22α or not. Scale bar, 10 μm. **f** qRT-PCR analysis of cholesterol intake (LDLR, SR-BI), efflux genes (ABCA1, ABCG1) and sclerosis related genes (Col1α, Eln) in WT and *Sm22α*$^{-/-}$ VSMCs incubated with or without cholesterol ($n = 3$). **g** The mRNA and protein levels of ABCA1 in WT and *Sm22α*$^{-/-}$ VSMCs treated with cholesterol for 0, 12, 24, 48, and 72 h, respectively ($n = 3$). **h** ORO staining of WT and *Sm22α*$^{-/-}$ VSMCs stimulated with cholesterol for 0, 24, 48, and 72 h, respectively, and quantification of positive ORO staining. Scale bar, 20 μm. **i** The binding activity of LXRα to the promoter of *abca1* gene was decreased in *Sm22α*$^{-/-}$ VSMCs ($n = 4$). **j** ChIP and RT-PCR detected LXRα binding to *col1α* promoter in WT and *Sm22α*$^{-/-}$ VSMCs ($n = 6$). **k** The Young's modulus of WT and *Sm22α*$^{-/-}$ VSMCs treated with or without cholesterol ($n = 120$). Data and images are representative of at least three independent experiments. Data in **a**, **g**, and **h** were analyzed by Kruskal–Wallis rank sum test and two-way ANOVA. Data in **b**, **c**, **f**, **i**, and **j** were analyzed by unpaired *t*-test. N.S. not significantly different; *$p < 0.05$; **$p < 0.01$; ***$p < 0.001$; ****$p < 0.0001$.

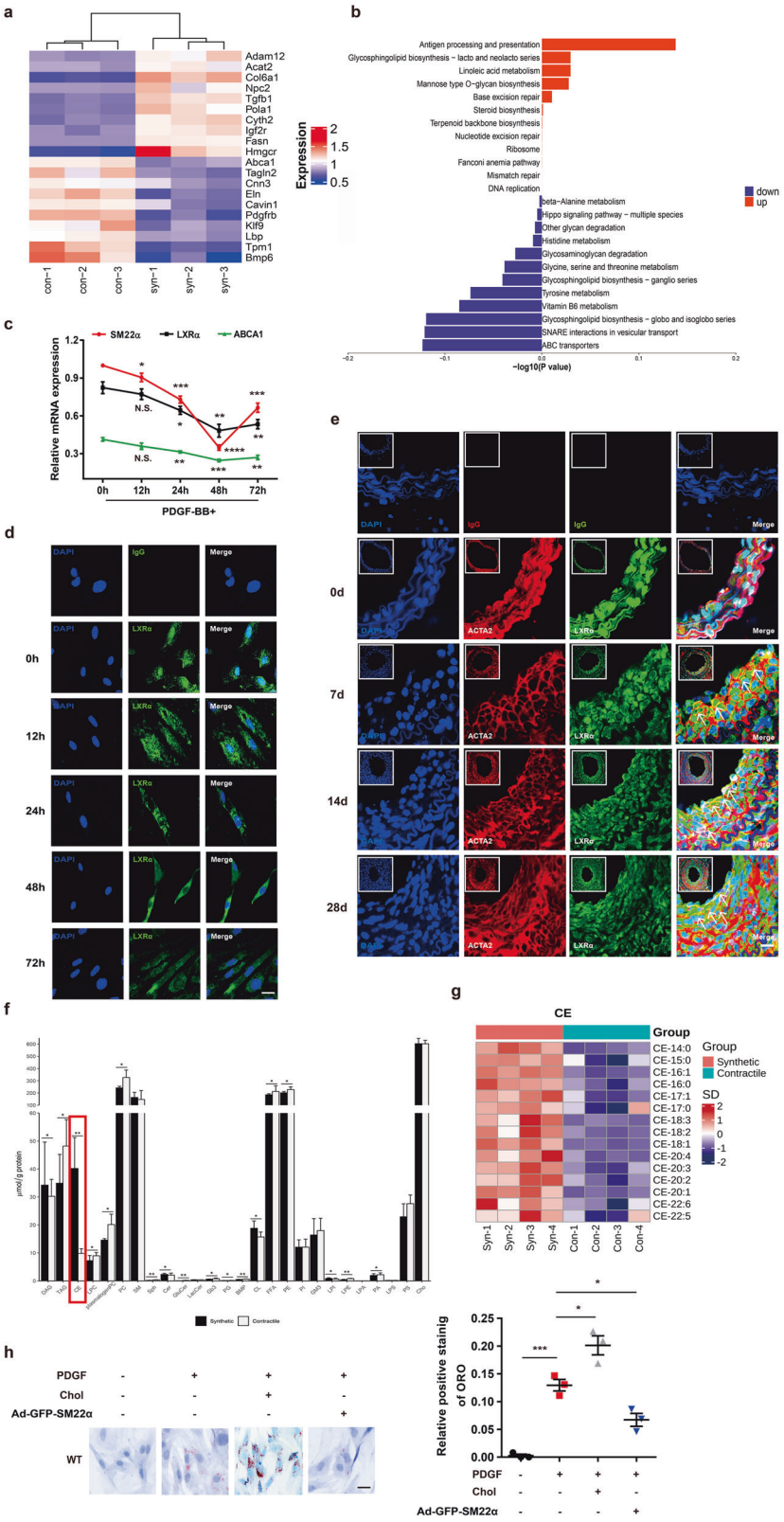
a
Adam12
Acat2
Col6a1
Npc2
Tgfb1
Pola1
Cyth2
Igf2r
Fasn
Hmgcr
Abca1
Tagln2
Cnn3
Eln
Cavin1
Pdgfrb
Klf9
Lbp
Tpm1
Bmp6
con−1
con−2
con−3
syn−1
syn−2
syn−3
Expression
2
1.5
1
0.5
b
Antigen processing and presentation
Glycosphingolipid biosynthesis − lacto and neolacto series
Linoleic acid metabolism
Mannose type O−glycan biosynthesis
Base excision repair
Steroid biosynthesis
Terpenoid backbone biosynthesis
Nucleotide excision repair
Ribosome
Fanconi anemia pathway
Mismatch repair
DNA replication
beta−Alanine metabolism
Hippo signaling pathway − multiple species
Other glycan degradation
Histidine metabolism
Glycosaminoglycan degradation
Glycine, serine and threonine metabolism
Glycosphingolipid biosynthesis − ganglio series
Tyrosine metabolism
Vitamin B6 metabolism
Glycosphingolipid biosynthesis − globo and isoglobo series
SNARE interactions in vesicular transport
ABC transporters
down
up
−log10(P value)
c
SM22α
LXRα
ABCA1
Relative mRNA expression
N.S.
0h
12h
24h
48h
72h
PDGF-BB+
d
DAPI
IgG
Merge
LXRα
0h
12h
24h
48h
72h
e
DAPI
IgG
Merge
ACTA2
LXRα
0d
7d
14d
28d
f
μmol/g protein
Synthetic
Contractile
g
CE
Group
CE-14:0
CE-15:0
CE-16:1
CE-16:0
CE-17:1
CE-17:0
CE-18:3
CE-18:2
CE-18:1
CE-20:4
CE-20:3
CE-20:2
CE-20:1
CE-22:6
CE-22:5
Synthetic
Contractile
SD
Syn-1
Syn-2
Syn-3
Syn-4
Con-1
Con-2
Con-3
Con-4
h
PDGF
Chol
Ad-GFP-SM22α
WT
Relative positive staining of ORO

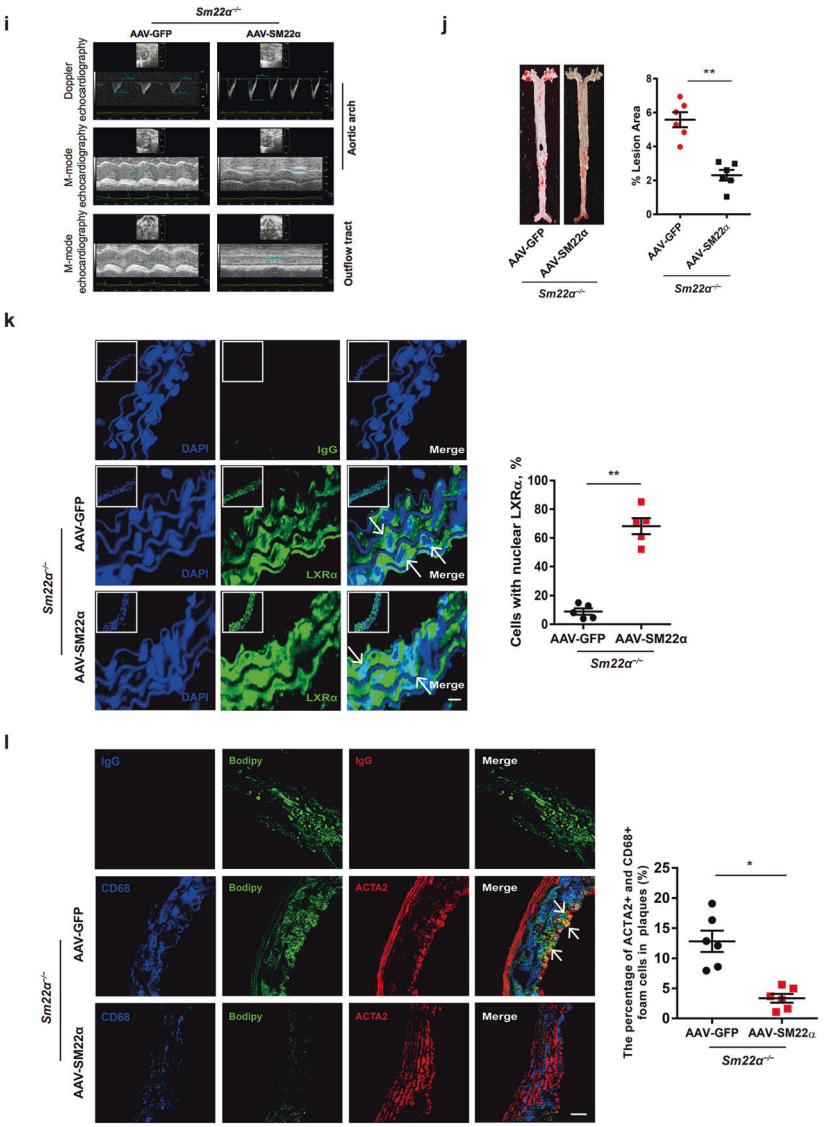

Fig. 3 Function of LXRα-ABCA1 axis is impaired in phenotypically switched VSMCs. a Heatmap of proteomic analysis between synthetic and contractile VSMCs. **b** Analysis of KEGG pathway enriched by differentially expressed genes of proteomic analysis between synthetic and contractile VSMCs. **c** The mRNA expression of SM22α, LXRα, and ABCA1 in WT VSMCs treated with PDGF-BB for 0, 12, 24, and 48 h, respectively ($n = 3$). **d** Confocal microscopy images of LXRα distribution in WT VSMCs incubated with PDGF-BB for 0, 12, 24, and 48 h, respectively. Scale bar, 10 μm. **e** Confocal microscopy images of LXRα and ACTA2 in arterial walls of WT mice after ligation for 0, 7, 14, and 28 days. Scale bar, 20 μm. **f** Quantification of each lipid class in synthetic and contractile VSMCs. Lipid classes were expressed as μmol per g protein. **g** Heatmap of CEs between synthetic and contractile VSMCs. **h** ORO staining of WT VSMCs transducted with or without Ad-GFP-SM22α following with PDGF-BB and/or cholesterol treatment and quantification of positive ORO staining. Scale bar, 20 μm ($n = 3$). **i** M-mode and Doppler echocardiography images obtained from aortic arch and outflow tract of $Sm22a^{-/-}$ mice transducted with AAV-GFP ($n = 10$) and AAV-SM22α ($n = 10$) fed Paigen diet for 12 weeks. A_s: outflow tract and aortic diameter in systole; A_d: outflow tract and aortic diameter in diastole. **j** Representative images of en face ORO-stained aortas and quantification of lesion areas ($n = 6$). **k** Representative immunofluorescence of LXRα (green) and quantification of cells with nuclear LXRα in the aortic sections from $Sm22a^{-/-}$ mice transducted with AAV-GFP ($n = 4$) and AAV-SM22α ($n = 4$) fed Paigen diet for 24 weeks. Scale bar, 10 μm. Arrows indicated the distribution of LXRα. **l** Identification of SMC-derived foam cells within atherosclerotic lesion of $Sm22a^{-/-}$ mice infected with AAV-GFP ($n = 4$) and AAV-SM22α ($n = 4$) fed Paigen diet for 24 weeks by CD68 (blue), ACTA2 (red), and Bodipy (green). Scale bar, 25 μm. Arrows indicated foam cells which were VSMCs-derived. Data and images are representative of at least three independent experiments. Data in **c** were analyzed by two-way ANOVA. Data in **f**, **h**, **j**, **k**, and **l** were analyzed by unpaired *t*-test. *$p < 0.05$; **$p < 0.01$; ***$p < 0.001$; ****$p < 0.0001$.

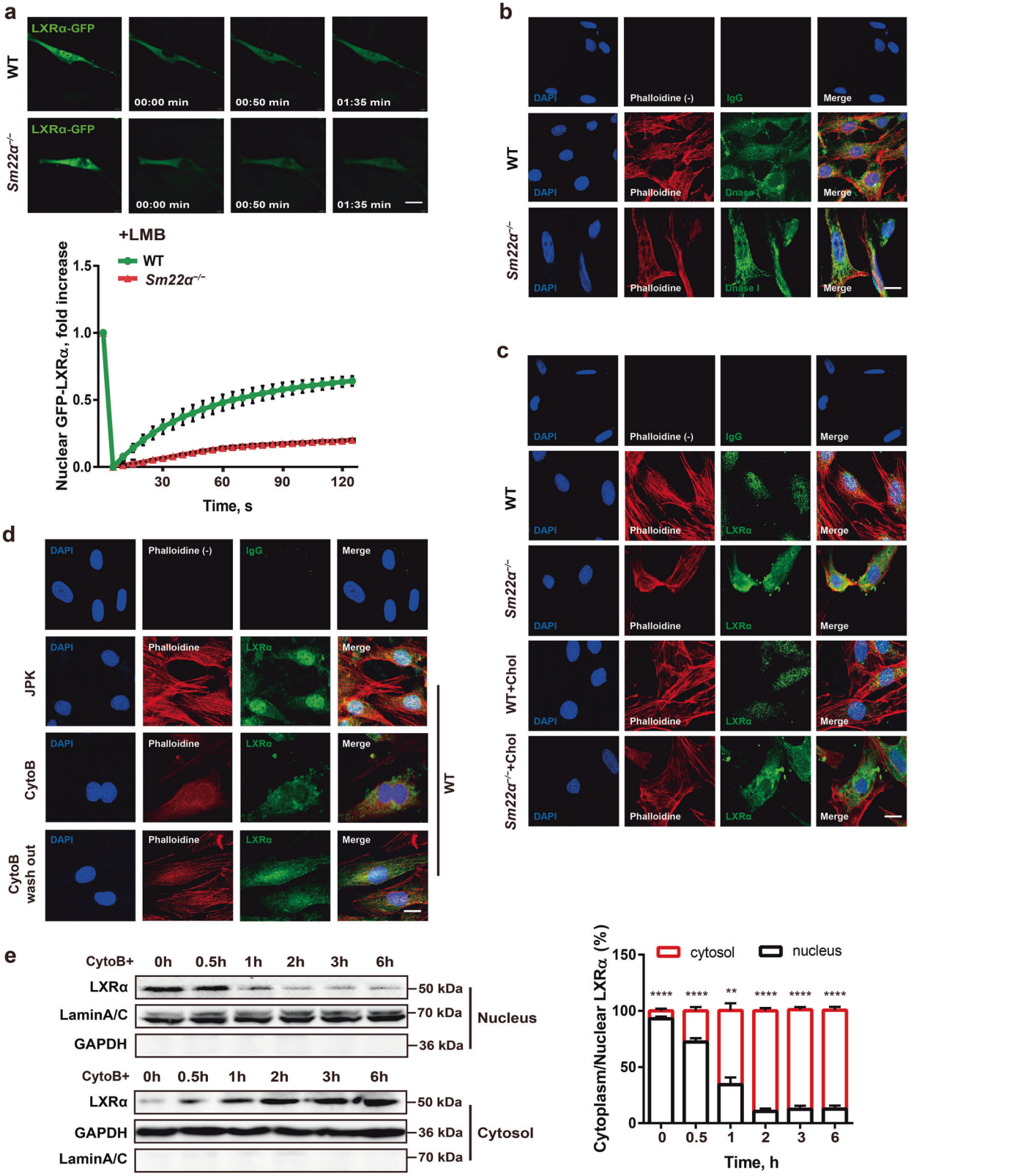

Fig. 4 Nuclear import of LXRα is regulated by actin dynamics. a Fluorescence recovery after photobleaching (FRAP) studies with LXRα-GFP to measure nuclear import. Cells were pretreated with LMB. Decreased accumulation of nuclear fluorescence indicates a lower rate of nuclear import of LXRα-GFP in *Sm22α*$^{-/-}$ VSMCs relative to WT controls ($n = 25$). **b** Representative images of F-actin (phalloidin, red) and G-actin (Dnasel, green) in WT and *Sm22α*$^{-/-}$ VSMCs. Scale bar, 10 μm. **c**, **d** Representative images for F-actin (phalloidin, red) and LXRα (green) in WT and *Sm22α*$^{-/-}$ VSMCs with cholesterol loading or not (**c**) and in WT VSMCs treated with JPK, CytoB and after CytoB washout (**d**). Scale bars, 10 μm. **e** Western blot analysis of cytoplasmic and nuclear LXRα in WT VSMCs treated with CytoB at different time points ($n = 6$). Data and images represent at least three independent experiments. Statistical analyses, unpaired *t*-test and Kruskal–Wallis rank sum test. $^{**}p < 0.01$; $^{***}p < 0.001$; $^{****}p < 0.0001$.

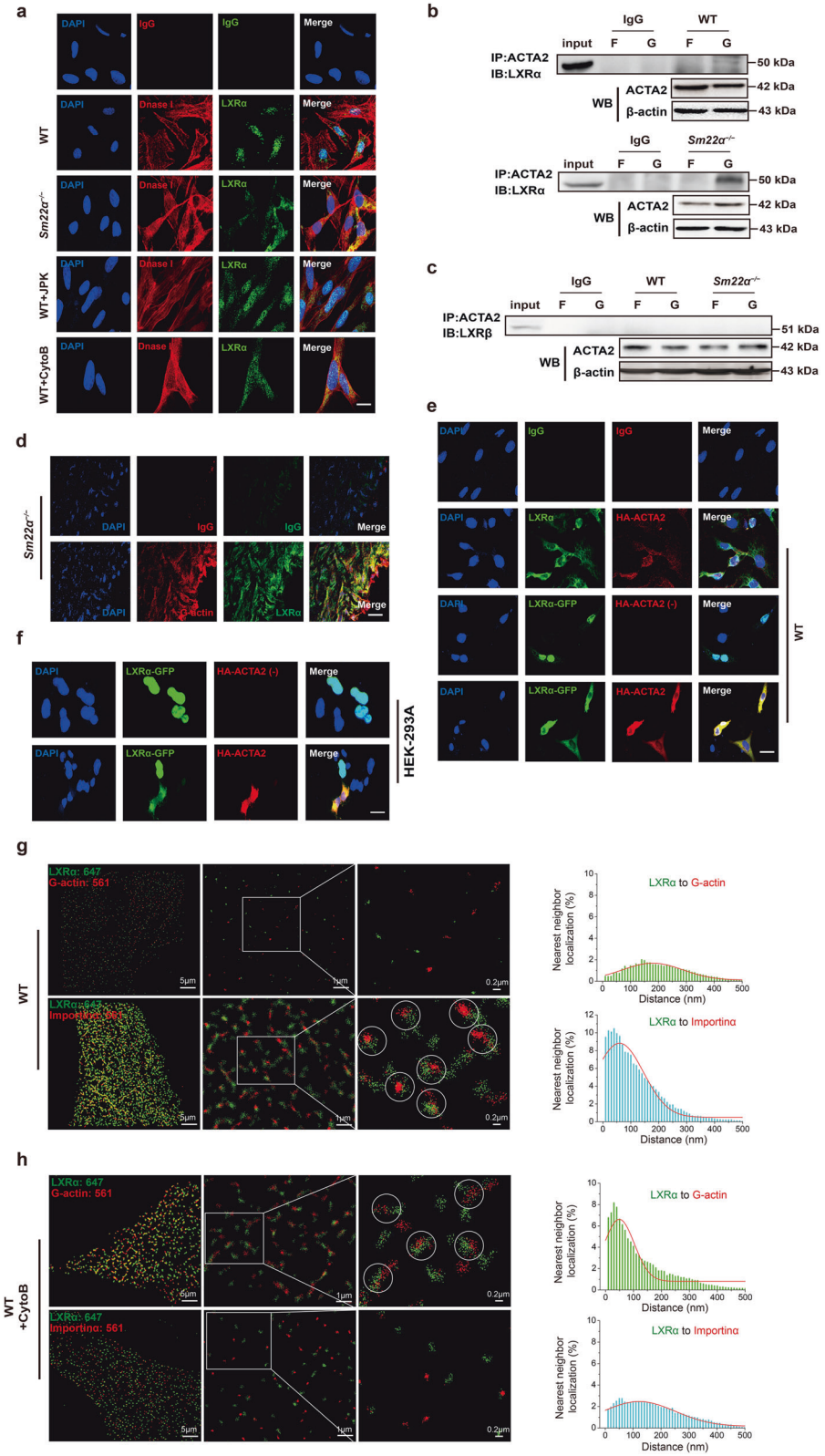
a
DAPI
IgG
IgG
Merge
WT
Dnase I
LXRα
Sm22α-/-
WT+JPK
WT+CytoB
b
IgG
WT
input
F
G
IP:ACTA2
IB:LXRα
50 kDa
WB
ACTA2
42 kDa
β-actin
43 kDa
Sm22α-/-
c
IP:ACTA2
IB:LXRβ
51 kDa
d
G-actin
e
HA-ACTA2
HA-ACTA2 (-)
LXRα-GFP
f
HEK-293A
g
LXRα: 647
G-actin: 561
Importinα: 561
5μm
1μm
0.2μm
LXRα to G-actin
LXRα to Importinα
Nearest neighbor localization (%)
Distance (nm)
h
WT +CytoB

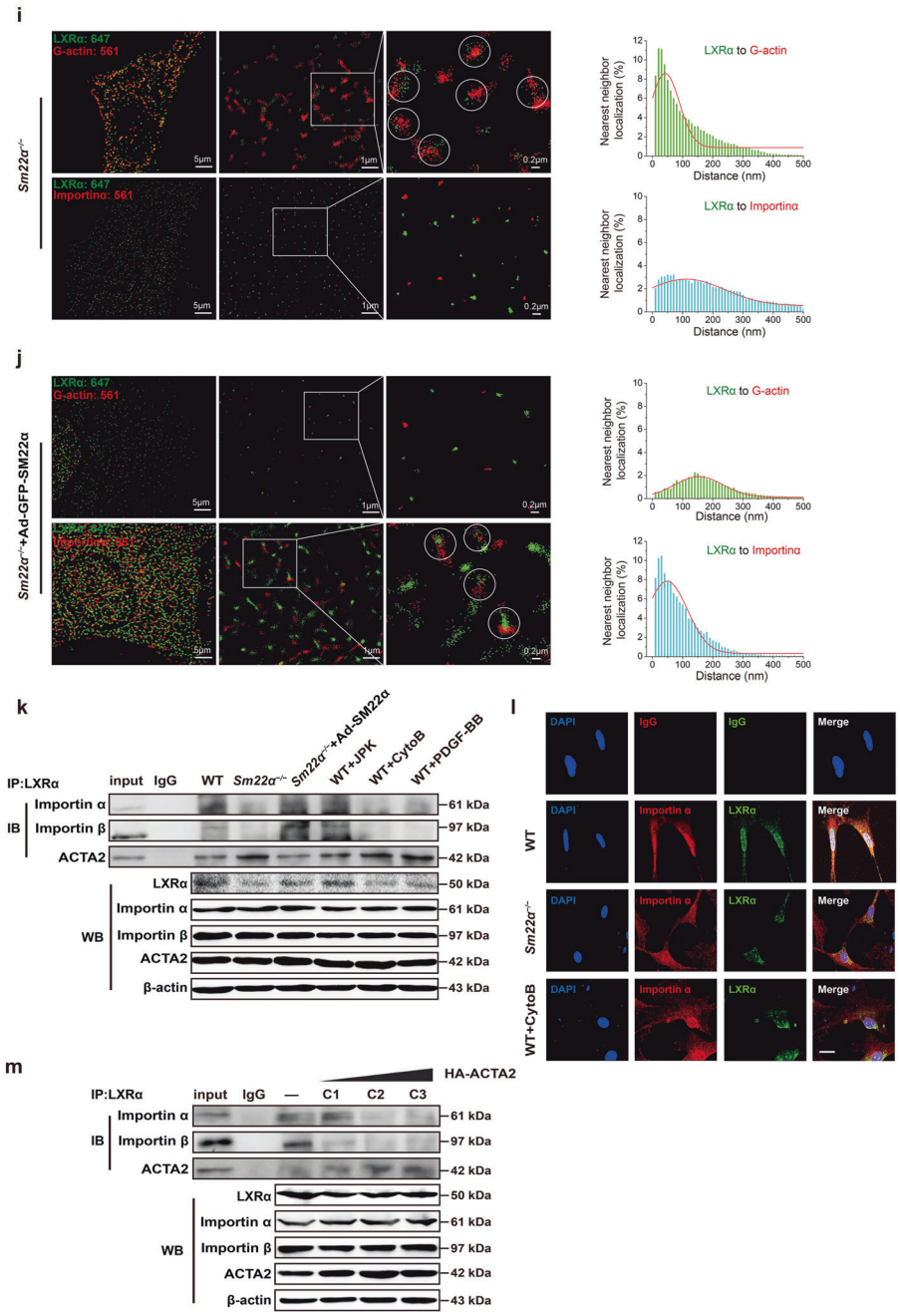

Fig. 5 G-actin interacts with and retains LXRα in the cytoplasm, blocking LXRα binding to Importin α. a Double immunofluorescence staining for G-actin (Dnasel, red) and LXRα (green) in WT VSMCs accompanied with treatment of JPK or CytoB and also in *Sm22α*$^{-/-}$ VSMCs. Scale bar, 10 μm. **b**, **c** Co-immunoprecipitation of ACTA2 and LXRα (**b**) and LXRβ (**c**), respectively, in F- and G-actin fractions of WT and *Sm22α*$^{-/-}$ VSMCs ($n = 3$). **d** Double immunofluorescence staining of G-actin (Dnase1, red) and LXRα (green) or IgG in atherosclerotic lesion in aortic wall of *Sm22α*$^{-/-}$ mice. Scale bar, 20 μm. **e** Representative immunofluorescence staining for endogenous LXRα (green) and LXRα-GFP (green) in WT VSMCs transfected with HA-ACTA2 (red, stained by anti-HA antibody) or not. Scale bar, 15 μm. **f** Representative immunofluorescence staining for LXRα-GFP (green) and HA-ACTA2 (red, stained by anti-HA antibody) in HEK-293A cells. Scale bar, 10 μm. **g**–**j** Two-color STORM images and quantification of the co-localization degree between LXRα and G-actin as well as Importin α in WT VSMCs with (**h**) or without (**g**) CytoB treatment and *Sm22α*$^{-/-}$ VSMCs with (**j**) or without (**i**) Ad-GFP-SM22α infection ($n > 10$). **k** Co-immunoprecipitation of LXRα and Improtin α, Improtin β or ACTA2 in WT and *Sm22α*$^{-/-}$ VSMCs with or without JPK, CytoB, PDGF-BB, and Ad-GFP-SM22α treatment ($n = 3$). **l** Double immunofluorescence staining for Importin α (red) and LXRα (green) in WT and *Sm22α*$^{-/-}$ VSMCs as well as CytoB-treated WT VSMCs. Scale bar, 15 μm. **m** Co-immunoprecipitation of LXRα and Importin α, Improtin β or ACTA2 in WT VSMCs transfected with HA-ACTA2 of different concentration ($n = 3$). Data and images represent at least three independent experiments.

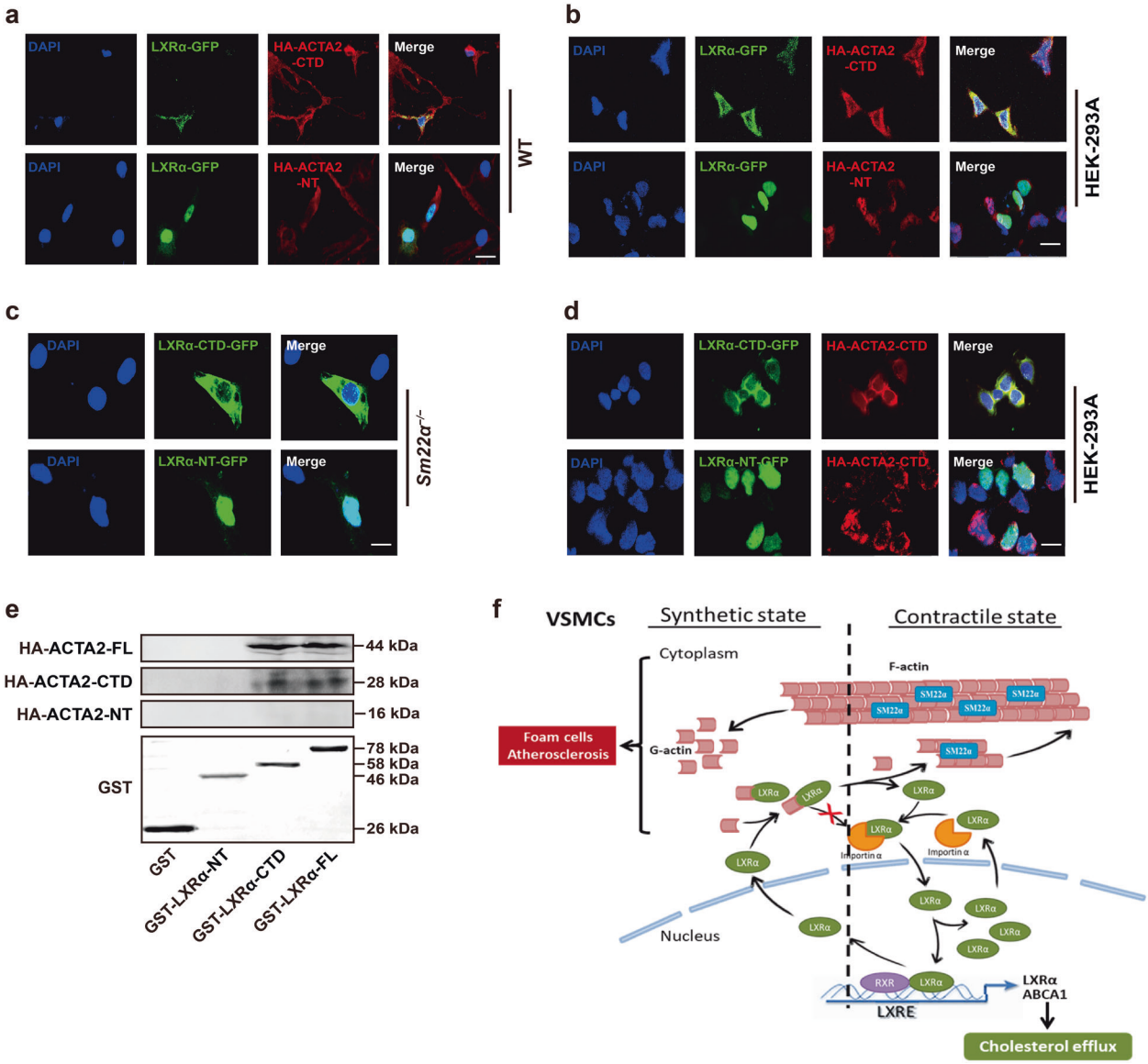

Fig. 6 The C-terminal domain mediates interaction between G-actin and LXRα. a Representative immunofluorescence staining for LXRα-GFP (green) in WT VSMCs transfected with HA-ACTA2-CTD (red) or HA-ACTA2-NT (red). Scale bar, 15 μm. **b** Representative immunofluorescence staining for LXRα-GFP (green) and HA-ACTA2-CTD (red) or HA-ACTA2-NT (red) in HEK-293A cells. Scale bar, 15 μm. **c** LXRα-CTD-GFP (green) or LXRα-NT-GFP (green) was transfected into *Sm22α*$^{-/-}$ VSMCs. Scale bar, 10 μm. **d** LXRα (-CTD, -NT)-GFP (green) and HA-ACTA2-CTD (red) were co-expressed in HEK-293A cells. Scale bar, 10 μm. **e** Interaction of HA-ACTA2 (-FL, -CTD, -NT) and GST-LXRα (-FL, -CTD, -NT) proteins analyzed by in vitro pull-down assay ($n = 3$). **f** Schematic representation of a working model which SM22α inhibits VSMC-derived foam cell formation by blocking actin-LXRα signaling ameliorating atherosclerosis. Data and images represent at least three independent experiments.